# Geothermal Hydrogen Well Modelling

Severinsen I[1], Talpas S[1], Payne J[1], Yu W[1] and Young B[1]

[1] Department of Chemical and Materials Engineering, University of Auckland, Auckland, New Zealand

isev820@aucklanduni.ac.nz

**Keywords:** *Geothermal hydrogen well, renewable energy, green hydrogen, wellbore modelling*

## ABSTRACT

A geothermal hydrogen well is a potential renewable energy solution to utilise otherwise unused geothermal or hydrocarbon wells as a passive source of hydrogen. This solution uses thermoelectric generators (TEG) to produce high current, low voltage electricity *in situ*. The electrical current is also used *in situ* to produce hydrogen through electrolysis of water. The solution is circulated in a coaxial borehole heat exchanger (CBHE) with the electrolyser situated in the annulus. This circulating fluid is necessary for electrolysis but also removes unwanted heat from the TEG and electrolyser. This work describes the developed solution and accompanying model in detail. A one-dimensional ordinary differential equation is used to simulate the heat transfer from the reservoir through the TEG, electrolysis and CBHE sections, predicting power and hydrogen production along the length of the well. An optimisation is performed to maximise hydrogen production rate while minimising parasitic pump and cooling tower power.

## 1. INTRODUCTION

### 1.1 Geothermal Energy

Conventional geothermal fields are unevenly geographically distributed, limited predominantly to volcanically active regions on plate boundaries or hot spots. Areas in geologically more stable regions have lower heat flow, but still can, to a lesser degree, be used for harnessing geothermal energy. An example of this is oil and gas extraction from reservoirs, as these tend to be heated to some degree from natural geothermal heat. In most cases, this is not utilised as the heat is of low grade - but utilisation of this heat is being investigated (Coronado Trivino et al., 2021).

### 1.2 Thermoelectric Materials

Thermoelectric materials are materials with a specific crystalline structure that induces a flow of charge in the presence of a temperature gradient. These semiconductor-like materials induce a concentration of charge carriers (e.g., electrons) at either hot or cold ends of a material with a thermal gradient. When p-type and n-type thermoelectric materials are arranged in an alternating arrangement, a device that generates power from heat without moving parts is formed (Mulla & Dunnill, 2019). These thermoelectric generators (TEG) are a mature design, with a notable example being the nuclear powered TEG used in the Voyager probes in 1977 (Rowe, 1991).

In modern times TEG have been proposed as a source of power for remote and essential operations. Under these conditions, a solid-state generator is beneficial despite the low efficiencies of such designs. A more recently proposed use case is generation of power for wearable electronics using the human body's heat (Nozariasbmarz et al., 2020). Large scale and industrial electricity production from heat focuses upon organic Rankine cycles as the preferred technology as efficiencies are typically higher than those seen with TEG (Champier, 2017).

### 1.3 Water electrolysis

Electrolysis of water to form hydrogen and oxygen is a mature technology. Alkaline and PEM electrolysis are commercially viable and are under considerable research scrutiny, with new catalyst designs the focus of much research (e.g., Grigoriev et al., 2020). Alkaline electrolysis is a more mature technology but favours more stable operation and has low efficiencies. PEM electrolysis is the design of choice for large scale where electricity cost is significant and frequent maintenance is possible - it also handles transient loads much better than alkaline electrolysis.

Modern electrolysis designs universally use a multitude of electrolysis cells connected in series, termed a stack. This means the required power for a stack has a high voltage and low current, and this reduces the losses from higher ohmic resistance. This design, while efficient, is inflexible in geometry, especially in constrained systems. Additionally, it is unsuitable for the rare case where the voltage and current are unable to be transformed using electrical equipment.

### 1.4 Geothermal Hydrogen Well

The developed geothermal hydrogen well design resembles a coaxial borehole heat exchanger (CBHE). Heat is extracted from the reservoir using an injected cold fluid, and the primary heat transfer is between this fluid and the reservoir through the casing and cement of the well. This design varies from the traditional CBHE in that it incorporates a TEG layer between the cold fluid and the reservoir generating power, similar to that described in Liu et al., (2020). The power from this layer is utilised in a hydrogen electrolyser within the flowing fluid. A CAD design of the system is shown in Figure 1.

In comparison to the traditional design, incorporating a TEG adds layers between the reservoir and the fluid flow reducing the area available for fluid flow. This increases pressure drop within the system by increasing the fluid's velocity. In addition, the TEG layer is intentionally an extremely poor thermal conductor. This means the temperature difference between the reservoir and fluid can be maintained which is the driving force for power production through the TEG.

Technical implementation of the TEG layer has significant challenges. Most notably the material between the TEG elements will need to be identified - traditionally this is air, but as the casings provide a pressurised environment, a vacuum could be used to prevent thermal short circuiting of the TEG. This vacuum could be maintained if the pipe segments are plumbed to the surface where a vacuum pump would be situated. Alternatively, each segment could be sealed with a vacuum in place. Additionally, implementing a thermally conductive, electrically nonconductive layer (typically Al2O3) between the casing and copper layer will also prove challenging.

The electrolyser is implemented as a connection between the inner tube downcomer and the main wall of the casing. This provides two functions: to separate the hydrogen and oxygen


ISSN 2703-4275

forming sides of the zero-gap electrolyser, and to increase surface area without compromising heat exchange area on the casing wall. A PTFE barrier is also employed opposite the electrolyser to fully isolate the hydrogen and oxygen rich streams within the annulus.

The electrolyser design utilised is an alkaline zero gap design. This is used because the opportunities for maintenance in this design are effectively none, and a resilient design is required. The electrical connection between the electrolyser current collectors and the TEG layer is simple, with copper elements extending from within the casing to the electrolyser itself. Appropriate sealing is required however, to isolate the electrically conductive copper from the fluid and isolate the vacuum gaps within the TEG from the high pressure fluid within the annulus.

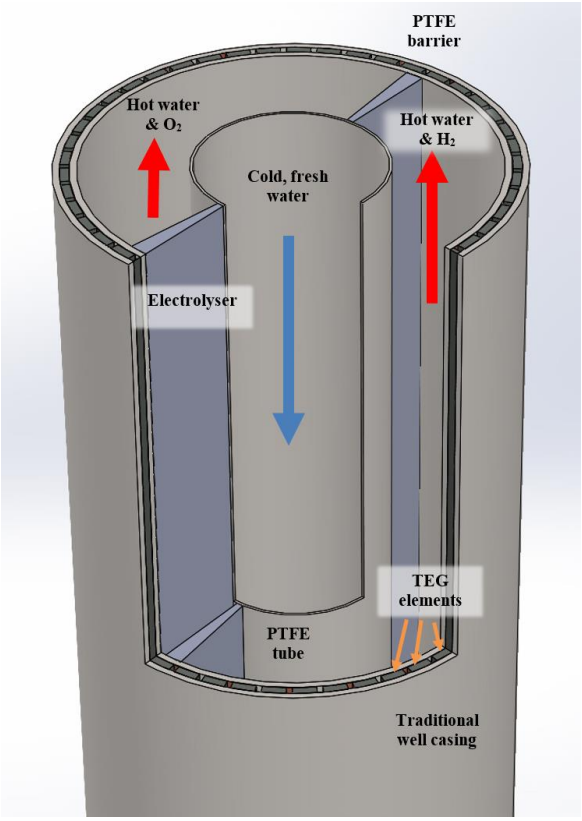


**Figure 1: CAD model of geothermal hydrogen well.**

## 2. METHODOLOGY

### 2.1 Existing well designs

The geothermal hydrogen well designed is intended to be used in existing wells. Thus, a typical design of a geothermal well was adopted as a basis for calculations. Two different typical well dimensions were used, as given in Sadiq J. Zarrouk & Katie McLean, (2019). The thermal gradient of the geothermal well used is specified as a bottomhole temperature of 295°C and a surface temperature of 30°C as given in Tonkin et al., (2021).

This basis of calculation addresses the use case where a geothermal well is repurposed into a hydrogen production device. An alternative use case is repurposing an oil and gas well, but this is beyond the scope of this work.

### 2.2 Heat transfer modelling

The model developed primarily concerns heat transfer from the reservoir to the circulating fluid. This is modelled as ordinary differential equations (ODE) for each layer between the reservoir and the circulating fluid. The generic equation for a primary heat transfer layer is shown in Equation (1). This derivative function is simply derived from a heat balance.

$$\frac{dT_j}{dz} = \frac{\left[U_{j-1}\pi d_{j-1}\left(T_{j-1} - T_j\right) - U_j\pi d_j\left(T_j - T_{j+1}\right)\right]}{m_j C_{p,j}} \quad (1)$$

where $U_j$ is the overall heat transfer coefficient for the j[th] layer, $T_j$ is the temperature of the j[th] layer, $d_j$ is the outer diameter of the j[th] layer, $m_j$ is the mass of the j[th] layer, and $C_{p,j}$ is the heat capacity of the j[th] layer.

For the TEG layer, an additional term is added in the numerator for the heat consumed and converted into electricity. For the circulating fluid the pressure is also tracked as an additional derivative using Equation 2.

$$\frac{dP}{dz} = \rho g - 0.5 f \frac{\rho u^2}{D_H} \quad (2)$$

where $\rho$ is the density of the fluid, $g$ is acceleration due to gravity, $f$ is the friction factor, $u$ is the fluids velocity, $D_H$ is the hydraulic diameter of the flow channel.

The convective heat transfer coefficient ($U$) is determined using the Dittius-Boehler correlation (Dittus & Boelter, 1985) and Gnielinski's correlation for annuli (Gnielinski, 2015). The friction factor ($f$) is determined using the Colebrook-White formula (Sonnad & Goudar, 2007). The inner tube temperature profile is then calculated using the calculated annulus temperature profile. From this the bottomhole temperature and pressure are determined, and the model iterated until the difference between iterations is below a specified tolerance.

During model development, various iterations of layers were incorporated into the model, including layers for thermal pastes between the main casing and TEG elements, as well as copper and $Al_2O_3$ layers within the TEG assembly. As these layers were sufficiently thin and thermally conductive, they did not improve the accuracy of the simulation and slowed calculations significantly - thus they were omitted.

There are significant assumptions made in the heat transfer model, including:

- Combining of layers, e.g., the TEG layer includes copper and $Al_2O_3$ layers as well as thermal and electrical interconnections.
- Heat transfer through the inter-element area within the TEG. This is considered as the spacing between elements is set and the number of elements is dynamically chosen such that the required voltage can be achieved. When the arrangement of elements is such that heat transfer through the inter-element space dominates the system operates as a simple insulation layer with air as the intermediary layer.
- The modelling of the system using ordinary differential equations for solids is somewhat flawed. As the model solves in the z dimension, each layer has a thermal mass that counteracts changes in temperature. This is not reflective of reality, as the system is at a steady state, and this means that all layers should have temperatures between the source (reservoir) and sink (annulus) temperatures. This assumes that axial conduction within each layer is insignificant, which is valid with the given dimensions of a well. The outcome of this is that when

the reservoir temperature reduces below the annulus temperature, some layers are resistant to changes in temperature and show non-source/sink layers as the layers with the highest temperatures. This was addressed by manually reducing the thermal mass of these layers - but this remains a limitation of this model.

- The annulus fluid is assumed to be water instead of a more complex solution for the purposes of thermal properties. When the required electrolysis voltage is calculated, the properties of the KOH solution are used.
- The impact of the hydrogen generated is not accounted for in the heat transfer. As the generated amounts are low this is not expected to have a significant impact on the bulk thermal properties or any possible two-phase flow regime.
- The reservoir is assumed to be an infinite heat source and changes to its temperature profile, as a result of utilisation, are not accounted for.

### 2.3 Thermoelectric modelling

The TEG module is modelled in tandem with the heat transfer model. Any power generated by the TEG will remove the same amount of heat via the heat transfer through the TEG layer. The generated voltage can be calculated by:

$$V_{TEG} = N_{elements}(\alpha_P - \alpha_N)(T_H - T_C) \quad (4)$$

where $N_{elements}$ is the number of thermoelements arranged circularly, $\alpha_P$ and $\alpha_N$ is the Seebeck coefficient of the p- and n- type thermoelements respectively and $T_C$ and $T_H$ are the temperatures of the cold and hot sides of the TEG module respectively.

The number of thermoelements used ($N_{elements}$) is calculated each iteration so that the TEG generates the appropriate voltage to sufficiently supply the electrolyser. This changes significantly as the temperature difference over the TEG deceases and the electrolyser required voltage drops.

The power generated is calculated using:

$$P_{TEG} = \dot{Q}_{in}\eta_{Carnot}\eta_{thermoelectric}$$
$$P_{TEG} = \dot{Q}_{in}\left(\frac{T_H - T_C}{T_H}\right)\left(\frac{\sqrt{1+ZT}-1}{\sqrt{1+ZT}+T_C/T_H}\right) \quad (5)$$

Where Q ̇_in is the heat flow through the TEG module, the dimensionless figure of merit ZT is defined by:

$$ZT = \frac{\alpha^2(T_H+T_C)}{2k\sigma} \quad (6)$$

where σ is the electrical resistivity of the thermoelectric material, k is the thermal conductivity of the thermoelectric material. Interestingly this means that producing power at a higher voltage minimally impacts the power produced. A higher voltage necessitates more thermoelectric elements which, in turn requires more inter-element spacing between the elements. This means a higher fraction of the heat transfer area is the insulating inter-element material which reduces heat transfer minimally, reducing power through Equation 5.

### 2.4 Electrolysis modelling

The electrolyser model uses the voltage and current inputs from the TEG model to calculate the hydrogen generated. The reversible voltage is first determined using the Nernst equation,

$$V_{rev} = V_{rev,0}(T) + \frac{RT}{2F}\ln\left(\frac{\left(P - P_{H_2O}\right)^{1.5}P^*_{H_2O}}{P_{H_2O}}\right) \quad (7)$$

where $T$ is temperature in K, $R$ is the gas constant, 8.314 J/molK, $F$ is Faraday's constant 96500 C/mol, $P$ is fluid pressure in Pa, $P_{H_2O}$ is partial pressure of $H_2O$ in Pa, $P^*_{H_2O}$ is saturated vapour pressure of $H_2O$ in Pa and $V_{rev}(T)$ is the standard reversible voltage as defined by Jang *et al*., (2021).

The activation losses are estimated using the Butler-Volmer equation, modified for the effect of bubble forming,

$$V_{act} = \frac{RT}{F\alpha_a}\left(\sinh^{-1}\left(\frac{j}{j_{0,a}}\right) - \sinh^{-1}(1-\theta)\right) + \frac{RT}{F\alpha_c}\left(\sinh^{-1}\left(\frac{j}{j_{0,c}}\right) - \sinh^{-1}(1-\theta)\right) \quad (8)$$

where $\alpha_a$ and $\alpha_c$ is the charge transfer coefficients of the anode and cathode respectively, $j$ is the current density in A/cm², $j_{0,a}$ and $j_{0,c}$ are the exchange current density of the anode and cathode respectively and $\theta$ is the covering coefficient. These parameters are defined in detail in Jang *et al*., (2021).

The ohmic losses are estimated using the known current and calculated resistances of the electrolyser's components,

$$V_{Ohm} = I\left(R_{cathode} + R_{anode} + R_{electrolyte} + R_{membrane}\right) \quad (9)$$

where $I$ is the current through the electrolyser in A and $R_j$ are the resistances of each layer respectively as defined by $R_j = d_j/(\sigma_j A_j)$, $d_j$ is the width of the layer, $A_j$ is the area of the layer and $\sigma_j$ is the electrical resistivity of the material $j$. These parameters are defined in detail in Jang *et al*., (2021).

The overall voltage required by the electrolyser is then calculated by:

$$V = V_{rev} + V_{act} + V_{Ohm}$$

If the supplied voltage from the TEG exceeds to required voltage, then electrolysis is predicted. Any overvoltage is converted into heat within the annulus fluid layer. This model does not account for side reactions occurring due to over/undervoltage. If electrolysis is predicted the rate of hydrogen production is calculated by,

$$\dot{m}_{H_2} = \frac{I}{2F}M_{H_2} \quad (10)$$

where $M_{H_2}$ is the molar mass of hydrogen in g/mol and $\dot{m}_{H_2}$ is the molar flowrate of hydrogen in g/s. A table of the parameter values used in the simulation is given in **Error! Reference source not found.**. Properties for the annulus fluid (water) are estimated using the CoolProp thermodynamic and fluid property package (Bell *et al*., 2014).

**Table 1. Table of parameter values used in the simulation**

| Parameter | Value | Unit | Reference |
|---|---|---|---|
| $L$ | 2217 | m | (Tonkin *et al*., 2021) |
| $dT/dz$ | 120 | K/m | (Tonkin *et al*., 2021) |
| $T_{bottomhole}$ | 295 | ℃ | (Tonkin *et al*., 2021) |
| $D_{cement}$ | 0.2572 | m | (Sadiq J. Zarrouk & Katie McLean, 2019) |
| $D_{ext\ casing}$ | 0.2445 | m | (Sadiq J. Zarrouk & Katie McLean, 2019) |
| $D_{TEG}$ | 0.2345 | m | - |
| $D_{int\ casing}$ | 0.2145 | m | - |
| $D_{annulus}$ | 0.2045 | m | - |
| $D_{inner\ tube,OD}$ | 0.15 | m | - |
| $D_{inner\ tube,ID}$ | 0.14 | m | - |


ISSN2703-4275

| | | | |
|---|---|---|---|
| $\rho_{cement}$ | 1830 | kg/m³ | (Song *et al.*, 2018) |
| $\rho_{casing}$ | 8060 | kg/m³ | (Song *et al.*, 2018) |
| $\rho_{PTFE}$ | 970 | kg/m³ | (Wang *et al.*, 2018) |
| $\rho_{TEG}$ | 7800 | kg/m³ | (Piggott, 2019) |
| $C_{p,cement}$ | 1900 | J/kgK | (Song *et al.*, 2018) |
| $C_{p,casing}$ | 400 | J/kgK | (Song *et al.*, 2018) |
| $C_{p,PTFE}$ | 2000 | J/kgK | (Wang *et al.*, 2018) |
| $C_{p,TEG}$ | 164.67 | J/kgK | (Piggott, 2019) |
| $k_{cement}$ | 3 | W/mK | (Liu *et al.*, 2020) |
| $k_{casing}$ | 45 | W/mK | (Liu *et al.*, 2020) |
| $k_{PTFE}$ | 0.068 | W/mK | (Liu *et al.*, 2020) |
| $k_{TEG}$ | 1.385 | W/mK | (Liu *et al.*, 2020) |
| $\sigma_P$ | $12.9 \times 10^{-6}$ | $\Omega/m$ | (Liu *et al.*, 2020) |
| $\sigma_N$ | $12.9 \times 10^{-6}$ | $\Omega/m$ | (Liu *et al.*, 2020) |
| $\alpha_P$ | $222.48 \times 10^{-6}$ | $V/K$ | (Liu *et al.*, 2020) |
| $\alpha_N$ | $-223.06 \times 10^{-6}$ | $V/K$ | (Liu *et al.*, 2020) |

## 3. RESULTS

The simulation was performed using the large sized well dimensions from Zarrouk and McLean, (2019). The remaining parameters specified are listed in Table 2 below.

**Table 2. Table of parameters used in the simulation.**

| Parameter | Value | Unit | Reference |
|---|---|---|---|
| $T_{top}$ | 50 | °C | - |
| $P_{top}$ | 50 | bar | - |
| $T_{bottomhole}$ | 295 | ℃ | (Tonkin *et al.*, 2021) |
| $\dot{m}_f$ | 30 | kg/s | - |

### 3.1 Thermal performance

Figure 2 shows that the insulated tube delivering cold fresh water to the bottom of the well works as intended, only

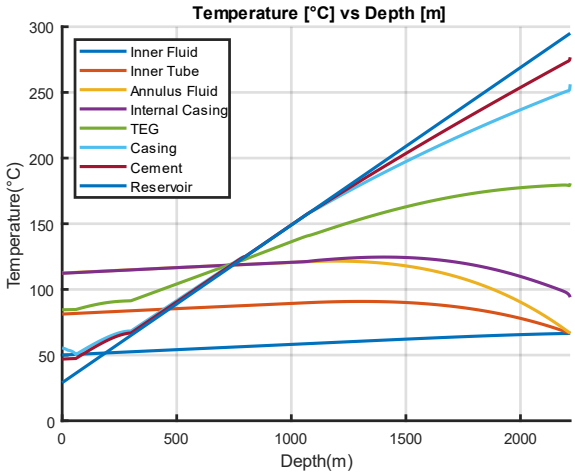


**Figure 1. Graph of temperature profiles of heat transfer layers over the depth of the well.**

increasing by 15°C down the entire depth of the well. As the water rises, it increases to ~120°C after 1000 m. At 750 m depth the reservoir and annulus fluid temperatures coincide and the axial temperature profiles invert. There is little change in temperatures at this point as the cement layer becomes very thick as the conductor and surface casing are encountered.

### 3.2 Hydrogen Production

**Error! Reference source not found.** shows the power generated by the TEG module is highly dependent upon the temperature difference across the TEG module. This is as predicted by Equations 5 and 6. The voltage required by the electrolyser is also shown in **Error! Reference source not found.**. The voltage generated exceeds the required voltage for most of the power generating length. This overvoltage is unlikely to induce side reactions within the system, as it is less than 0.1 V. This arises due to the order of calculation where the number of thermo-elements is estimated before the heat transfer profile at each depth is calculated, meaning it uses estimates from the previous step. When the heat transfer is dominated by heat flow through the inter-element material, the TEG layer becomes an insulating layer. This is seen at 1200 m in Figure 2. At this point the number of thermo-elements required is significant and, as seen in Figure 2, the power generated drops significantly by this point. Past the point where the temperature difference inverts at ~750 m depth, the insulation provided by the inter-element material is no longer beneficial. Past this point the well should be optimised for cooling as this reduces the need for significant cooling above ground.

Where electrolysis is possible, hydrogen is generated which

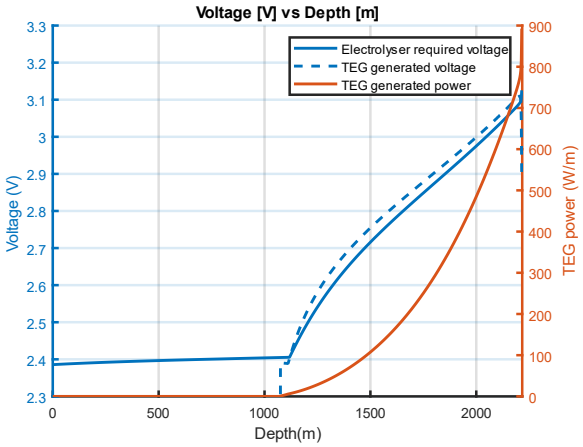


**Figure 3. Graph of power and voltage generated by the TEG as well as voltage required by the electrolyser.**

is shown in Figure 4. Here hydrogen production drops sharply in relation to changes in current, and voltage supplied, as well as changes to required voltage through increased temperatures and pressures of the circulating fluid.

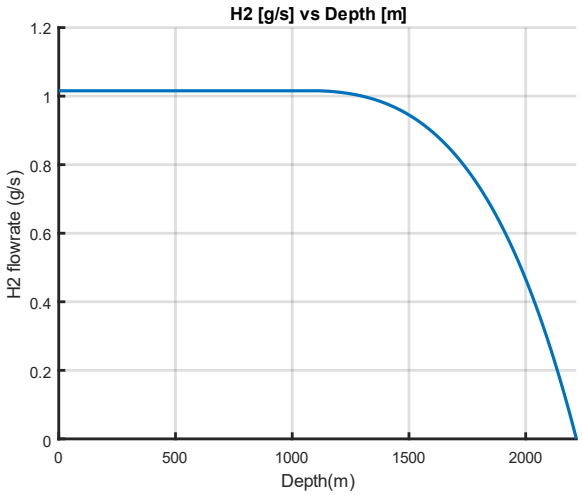


**Figure 2. Graph of hydrogen flowrate as a function of depth.**


ISSN2703-4275

### 3.3 Sensitivity Analysis

The system as shown has a variety of parameters that can be tuned to optimise the efficacy of the well. The most notable parameter is the flowrate of the circulating fluid. Changes in flowrate impact the frictional pressure drop within the system significantly, as well as the heat that must be rejected above ground to return the fluid to its inlet temperature. These two factors have been combined into a total parasitic power load upon the system. Increases in flowrate also impact the hydrogen generated, as the annulus stays at a lower temperature for longer, improving TEG power generated. These two metrics can be combined by tabulating the energy required per kg of hydrogen generated. This is shown in Figure 5, where it is compared against the theoretical electrical load upon a standard electrolyser.

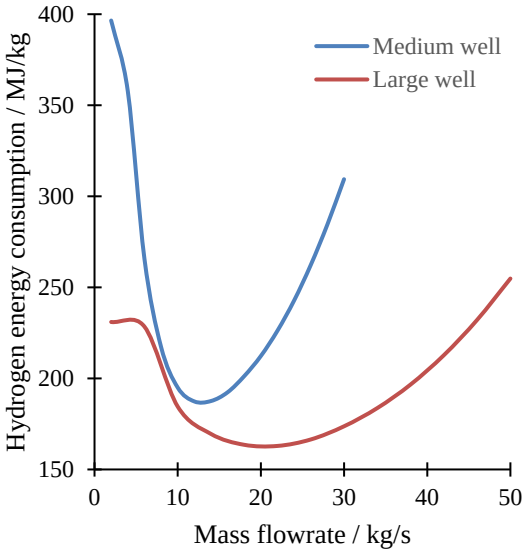


**Figure 3. Graph of electricity consumption per kg of hydrogen produced.**

Figure 5 shows that the most energy efficient operational regime varies with well diameter. Each individual size has an optimal flowrate starting at 25 kg/s for the largest well and reducing to 12 kg/s for the medium well. This is an expected result as low flowrates result in higher bottom hole temperatures meaning initial temperature difference over the TEG at the bottom of the hole is lower, meaning more thermocouples are required, reducing power production. At higher flowrates the benefits of colder temperatures for longer are overshadowed by the significantly increased pressure drop and associated increased pump power required.

## 4. DISCUSSION

This innovative solution helps reduce the electricity required to produce hydrogen, this is because the electricity required to run the well is disconnected from the electricity used for electrolysis. In many ways this can be thought of as an electrolyser with >100% efficiency, unfortunately to achieve this efficiency requires a significant capital cost and has a single operating point with no scalability or flexibility. This solution however is predicated on many factors that are rarely present in real situations. Firstly, a large diameter geothermal well must be drilled and secondly, the cost of hydrogen and electricity must be such that this solution is more feasible than a traditional extractive well with a surface electrolyser. This is possible if the well is unsuitable for extracting fluid for some reason, and in this case repurposing the well in this way may recoup costs compared to abandoning or repurposing the well. Unfortunately, this solution is still competing with hydrogen produced from fossil fuels, and even with an electricity consumption lower than current electrolysers the necessary sale price of hydrogen is $3.15/kg with a price of electricity of $70/MWh. Cheaper electricity prices are feasible with renewables like solar or wind but the systems residence time of 1 hour is relatively incompatible with such dynamic systems.

## 5. CONCLUSIONS

A novel clean energy solution is detailed in this work. The simulation performed captured many of the complexities of the system as described. The system simulated can generate hydrogen with a lower electricity consumption than a traditional electrolyser. Overall, the well can produce approximately 86 kg $H_2$/day using 161 kW instead of 188 kW if a traditional electrolyser was used. Various parameters of the system were altered to analyse the sensitivity of the system. It was found that the circulating fluid flowrate was a key parameter that impacted hydrogen production efficiency.

This investigation shows that this combination of technologies is technically feasible. Unfortunately, situating such a device at the bottom of a well causes such significant pressure drop and increased costs that such a solution is unlikely to be economic unless the cost of drilling the geothermal well is not considered. Additionally, the economics are highly sensitive to power price such that coupling this with an extremely cheap source of power could be feasible.

Future work could focus on improving various aspects of the model. This includes accounting for the response of the geothermal reservoir to non-extractive exploitation. Additionally, the comparison between a more traditional geothermal power generation and associated above ground electrolysis system should be incorporated. More consideration should be given to the coupled TEG and electrolyser design for utilisation of waste heat. Although for non-space constrained systems the ohmic losses will likely prove untenable when compared to transformation of the DC power into a higher voltage for traditional electrolysis.


ISSN2703-4275

**ACKNOWLEDGEMENTS**

We would like to acknowledge Ahuora (MBIE Advanced Energy Technology Strategic Science Investment Fund) and the University of Auckland doctoral scholarship support for funding.

**REFERENCES**

Bell, I. H., Wronski, J., Quoilin, S., & Lemort, V. (2014). Pure and pseudo-pure fluid thermophysical property evaluation and the open-source thermophysical property library CoolProp. *Industrial & Engineering Chemistry Research*, *53*(6), 2498–2508.

Champier, D. (2017). Thermoelectric generators: A review of applications. *Energy Conversion and Management*, *140*, 167–181. https://doi.org/10.1016/j.enconman.2017.02.070

Coronado Trivino, C., Yu, W., Severinsen, I. L., Van Campen, B., & Young, B. R. (2021, November 23). Techno-economic estimation of the geothermal potential of existing Colombian oilfield production wells. *Proceedings 43rd New Zealand Geothermal Workshop*. New Zealand Geothermal Workshop, Wellington, New Zealand.

Dittus, F. W., & Boelter, L. M. K. (1985). Heat transfer in automobile radiators of the tubular type. *International Communications in Heat and Mass Transfer*, *12*(1), 3–22.

Gnielinski, V. (2015). Turbulent Heat Transfer in Annular Spaces—A New Comprehensive Correlation. *Heat Transfer Engineering*, *36*(9), 787–789. https://doi.org/10.1080/01457632.2015.962953

Grigoriev, S. A., Fateev, V. N., Bessarabov, D. G., & Millet, P. (2020). Current status, research trends, and challenges in water electrolysis science and technology. *International Journal of Hydrogen Energy*, *45*(49), 26036–26058. https://doi.org/10.1016/j.ijhydene.2020.03.109

Jang, D., Cho, H.-S., & Kang, S. (2021). Numerical modeling and analysis of the effect of pressure on the performance of an alkaline water electrolysis system. *Applied Energy*, *287*, 116554. https://doi.org/10.1016/j.apenergy.2021.116554

Korenaga, J. (2011). Clairvoyant geoneutrinos. *Nature Geoscience*, *4*(9), 581–582. https://doi.org/10.1038/ngeo1240

Liu, J., Wang, Z., Shi, K., Li, Y., Liu, L., & Wu, X. (2020). Analysis and modeling of thermoelectric power generation in oil wells: A potential power supply for downhole instruments using in-situ geothermal energy. *Renewable Energy*, *150*, 561–569. https://doi.org/10.1016/j.renene.2019.12.120

Mulla, R., & Dunnill, C. W. (2019). Powering the Hydrogen Economy from Waste Heat: A Review of Heat-to-Hydrogen Concepts. *ChemSusChem*, *12*(17), 3882–3895. https://doi.org/10.1002/cssc.201901426

Nozariasbmarz, A., Collins, H., Dsouza, K., Polash, M. H., Hosseini, M., Hyland, M., Liu, J., Malhotra, A., Ortiz, F. M., Mohaddes, F., Ramesh, V. P., Sargolzaeiaval, Y., Snouwaert, N., Özturk, M. C., & Vashaee, D. (2020). Review of wearable thermoelectric energy harvesting: From body temperature to electronic systems. *Applied Energy*, *258*, 114069. https://doi.org/10.1016/j.apenergy.2019.114069

Piggott, A. (2019). Detailed Transient Multiphysics Model for Fast and Accurate Design, Simulation and Optimization of a Thermoelectric Generator (TEG) or Thermal Energy Harvesting Device. *Journal of Electronic Materials*, *48*(9), 5442–5452. https://doi.org/10.1007/s11664-019-06952-x

Rowe, D. M. (1991). Applications of nuclear-powered thermoelectric generators in space. *Applied Energy*, *40*(4), 241–271. https://doi.org/10.1016/0306-2619(91)90020-X

Sadiq J. Zarrouk & Katie McLean. (2019). *Geothermal Well Test Analysis: Fundamentals, Applications and Advanced Techniques*. Academic Press; eBook Collection (EBSCOhost). https://ezproxy.auckland.ac.nz/login?url=https://search.ebscohost.com/login.aspx?direct=true&db=nlebk&AN=1951588&site=ehost-live&scope=site

Song, X., Zheng, R., Li, G., Shi, Y., Wang, G., & Li, J. (2018). Heat extraction performance of a downhole coaxial heat exchanger geothermal system by considering fluid flow in the reservoir. *Geothermics*, *76*, 190–200. https://doi.org/10.1016/j.geothermics.2018.07.012

Sonnad, J. R., & Goudar, C. T. (2007). Explicit Reformulation of the Colebrook−White Equation for Turbulent Flow Friction Factor Calculation. *Industrial & Engineering Chemistry Research*, *46*(8), 2593–2600. https://doi.org/10.1021/ie0340241

Tonkin, R. A., O'Sullivan, M. J., & O'Sullivan, J. P. (2021). A review of mathematical models for geothermal wellbore simulation. *Geothermics*, *97*, 102255. https://doi.org/10.1016/j.geothermics.2021.102255

Wang, K., Liu, J., & Wu, X. (2018). Downhole geothermal power generation in oil and gas wells. *Geothermics*, *76*, 141–148. https://doi.org/10.1016/j.geothermics.2018.07.005


ISSN2703-4275